Advances in Science and Technology Research Journal

Advances in Science and Technology Research Journal 2024, 18(4), 336–346
https://doi.org/10.12913/22998624/188742
ISSN 2299-8624, License CC-BY 4.0

Received: 2024.04.04
Accepted: 2024.06.05
Published: 2024.06.20

Numerical Study of Rotary Friction Welding of Automotive Components

Wojciech Więckowski[1*], Piotr Lacki[2], Anna Derlatka[2], Paweł Wieczorek[3]

[1] Department of Technology and Automation, Czestochowa University of Technology, ul. Generała Jana Henryka Dąbrowskiego 69, 42-201 Czestochowa, Poland

[2] Department of Civil Engineering, Czestochowa University of Technology, Department of Technology and Automation, Czestochowa University of Technology, ul. Generała Jana Henryka Dąbrowskiego 69, 42-201 Czestochowa, Poland

[3] Department of Materials Engineering, Czestochowa University of Technology, Department of Technology and Automation, Czestochowa University of Technology, ul. Generała Jana Henryka Dąbrowskiego 69, 42-201 Czestochowa, Poland

* Corresponding author's e-mail: wojciech.wieckowski@pcz.pl

ABSTRACT

The aim of the research was to select a material from which a washer can be made, so that it can be connected to an E355 steel tube by Rotary Friction Welding (RFW). It was decided to choose the steel grade X6CrMo17-1. The numerical model of the RFW process was built using the finite element method (FEM) using the ADINA System software. The numerical model takes into account the friction coefficient with variable values depending on the temperature. Numerical simulations of the process made it possible to determine the temperature fields in the weld cross-section. For the assumed process parameters: rotational speed of 14,000 rpm, friction time of 1.5 s and friction force of 600 N, the peak temperature occurred in the middle of the friction surface at the end of the friction phase and amounted to 1050 °C. The results of the temperature analysis are one of the most important parameters for the implementation of subsequent calculations, such as the calculation of structural changes, hardness, residual stresses and deformations.

Keywords: automotive, FEM, friction welding, RFW.

INTRODUCTION

Friction welding is a solid-state joining process in which the heat necessary to make a permanent connection comes from the direct conversion of mechanical energy into thermal energy as a result of friction in the contact area of the welded components. The oldest and most widely used variant of friction welding is RFW, in which one of the welded element rotates around its own axis while the other is stationary [1–3].

An important advantage of the process is that the process of joining materials takes place in a solid state, thanks to which the joints are free of defects that arise during melting and solidification of the material, such as bubbles or cracks, and the deformation of the joints is limited. The lower temperature in the welding zone creates a narrow heat affected zone (HAZ) and limits the formation of brittle intermetallic compounds (IMC), which allows the joining of various materials with different physical properties that cannot be joined using conventional welding methods, such as: copper with aluminum, aluminum with steel, titanium with steel, etc. RFW allows you to connect objects of various shapes and dimensions (at least one of the joined element must have a circular cross-section in the welding area), such as: pipe with pipe, rod with rod, pipe with rod, pipe with disc, rod with plate, etc., without the need to use additional binder and shielding gases and special preparation of the joined surfaces. The ability to control and monitor process parameters

makes it easy to automate, resulting in high and repeatable quality of manufactured joints. Additionally, reduced energy consumption, reduced raw material costs and shortened production time ensure lower joint manufacturing costs compared to other welding technologies [4, 5].

Thanks to numerous advantages, RFW is widely used, e.g. in the engineering, automotive, aviation and medical industries [6, 7]. Thanks to the possibility of joining elements of various shapes, made of different materials, a wide range of metal components made by casting or plastic forming technology can be replaced with cheaper, more durable and lighter friction welded products. RFW is used, for example, to connect turbine shafts, elements of car parts (e.g. brake discs, drive shafts, valves), copper-aluminium electrical connections, elements of cutting tools (e.g. twist drills), for the production of implants, for making pipe joints, etc. [8–10].

One of the varieties of RFW is Continuous Drive Friction Welding (CDFW), where one of the welded elements is constantly driven by the machine's spindle motor. The RFW process takes place in two main stages (friction and upsetting), which can be further divided into sub-periods. First, there is a friction step during which one welded element is driven relative to the other to a rotational speed n under the action of an axial compressive force (friction force). The friction between the surfaces generates heat, causing the material to plasticize. The compressive force displaces the plasticized material from the contact surface, while removing the original layer of oxides and other impurities, thanks to which the joined surfaces will come into close contact. The plasticized material flows radially outward, creating the so-called flash. This phenomenon is accompanied by shortening of the workpieces in the direction of the clamping force. The rate of axial shortening in the friction phase, called the burn-off rate, is an important parameter with respect to which the time of the welding cycle is controlled. After the required burn-off step, the upsetting stage occurs, in which the rotational movement is stopped while the forging force is increased and maintained, in order to establish a metallic bond between the joined surfaces and constitute a durable weld [1, 3].

The basic parameters in the friction welding process: rotational speed – n, friction force – F_f, friction time – t_f, upset force – F_u, upset time – t_u and stopping time – t_s [3, 11]. Welding parameters are strongly interrelated and can vary in a wide range, depending on the type, shape and dimensions of the welded components and the expected properties of the weld. Balta et al. [10] presented the results of optimizing the parameters of the welding process of a tubular element made of DIN 2394-ERD9056 with a forged support made of AISI 1045. The relationship between the welding parameters (friction force, friction time, upset force, upset time) and the mechanical properties of the joint (continuous strength, elongation) was investigated using the response surface methodology (RSM).

The RFW parameters determine the amount of energy introduced into the welding area and the rate of heat generation, which affect the range and microstructure of the zones present in the weld area (WCZ – weld center zone, TMAZ – thermo-mechanically affected zone and HAZ – heat affected zone), which in turn affects the quality of the weld. Appropriately selected parameters of the RFW process allow to obtain joints with comparable or higher strength compared to the raw material. An important factor influencing the properties of the weld is also the cooling rate of the joint area after welding [12]. The selection of RFW welding parameters, especially in the case of joining different materials, is complicated and requires a series of experimental tests.

Murugan et al. [8] presented the results of testing RFW joints made of SS304 and AA6063 bars with a diameter of 12 mm, at constant process parameters (n =1300 rpm, friction pressure of 1.8 MPa, t_f= 5 s, upset pressure of 2.4 MPa, t_u= 3 s). The authors of the work examined the impact of the shape of the front surfaces of the joined components on the total shortening and strength properties of the joints.

The results of friction welding of tungsten bars with steel bars (S355) are presented in [13]. In order to eliminate the access of oxygen and shorten the heating time, the welding process was carried out in a protective atmosphere with a rotational speed of n = 10,000 rpm, with friction pressure of 110 MPa, t_f = 0.9 s, upset pressure of 137.5 MPa, t_u= 2 s. Quality of joints was assessed on the basis of hardness measurement in the joint cross-section and EDS-SEM analysis of the structure and chemical composition in the area of the joint.

An important role in the optimization of friction welding processes is played by numerical

simulations of the process using the finite element method. Simulations allow to determine the deformation distributions and temperature gradients in the welded elements components. Then, on their basis, the quality of the joints can be estimated. Numerical models of the process often make it possible to eliminate experimental tests, and thus significantly reduce the time and costs of the production preparation stage. The simulation of RFW process is a complex task, taking into account the phenomena of heat flow, contact and friction as well as the issues of large plastic deformations [14]. Hence an important aspect of RFW simulation is the method of discretization of the area and regeneration of distorted meshes [15].

The quality of the obtained simulation results is affected by the accuracy of mapping the real conditions of the process, including changes in the properties of the welded materials as a function of temperature and the adopted simplifications. The authors of paper [16], using FEM simulations, analysed the impact of the model of friction states adopted in the calculations on thermal phenomena in the RFW process of SUS30 stainless steel. A method for determining the basic parameters of rotational friction welding (RFW) based on the analysis of frictional heat transfer on faying surfaces was presented in [17]. For dissimilar Ti Grade 2/AA 5005 joints, the authors determined the optimal parameters of the welding process in order to obtain the assumed contact surface temperature to obtain a good-quality weld.

GOAL AND SCOPE OF WORK

The aim of the research was to select the material from which a washer can be made, so that it can be connected to a tube, and to select the parameters of the rotational friction welding process of these components. The scope of work included the development of a numerical model of the rotational friction welding process of components in the form of the tube made of E355 steel and the washer on shown in Figure 1. Selection of the stainless steel grade for the washer was made on the basis of the following assumptions: the microstructure should be ferritic and the yield strength must be at a level similar to that of E355 steel. The list of potential grades is shown in Figure 2. It was decided to choose the steel grade X6Cr-Mo17-1. Table 1 shows the chemical composition of the base materials.

The thermomechanical properties of the base materials before welding are presented in Table 2 and Table 3. For the welded materials, the dependence of the yield strength on temperature was defined, which was determined on the basis of the true strain – true stress relationship. The paper presents the results of numerical calculations of temperature distribution in welded elements for the assumed parameters of the welding process.

NUMERICAL MODEL

The numerical model of the RFW process was built using the finite element method

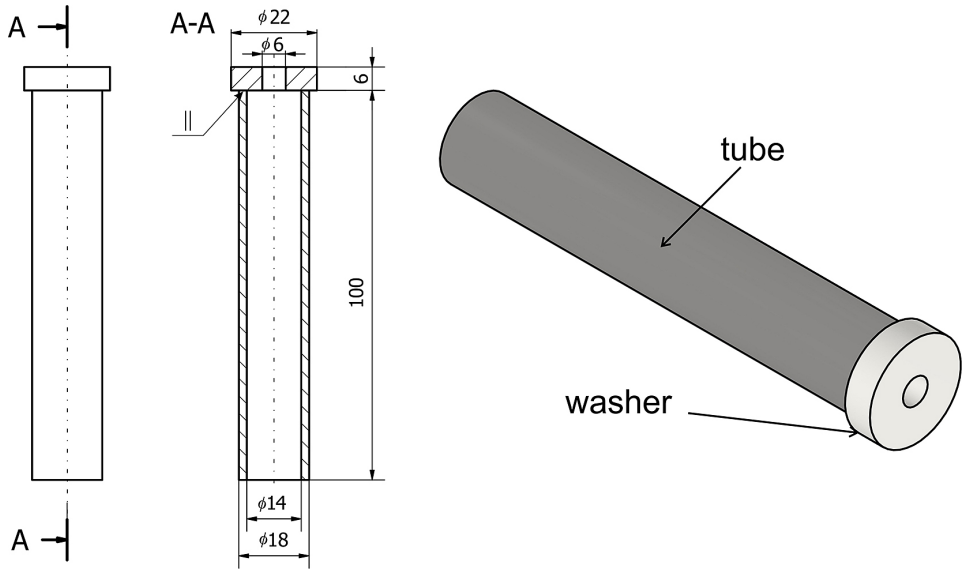

Figure 1. Shape and dimensions of welded parts

Table 1. Chemical composition of E355 and X6CrMo17-1 steel [18]

Element content (wt. %)						
E355 steel						
C	Mn		Si	P	S	
Max 0.22	Max 1.6		Max 0.55	Max 0.045	Max 0.045	
X6CrMo17-1 steel						
C	Si	Mn	P	S	Cr	Mo
Max 0.08	Max 1	Max 1	Max 0.04	Max 0.015	16–18	0.9–1.4

Table 2. Mechanical properties of base materials [18]

Material	Density, kg/m^3	Yield strength, MPa	Ulimate tensile strength, MPa	Young's modulus, GPa	Poissons ratio, -	Shear modulus, GPa
E355	7800	355	490	210	0.3	80
X6CrMo17-1	7700	350	500	200	0.28	78

Table 3. Thermal properties of base materials [18]

Material	Melting point, °C	Thermal condutivity, W/mK	Themal expansion, 10^{-6}/K	Specific heat capacity, J/KgK
E355	1370–1400	42	16	470
X6CrMo17-1	1430–1510	25	10	475

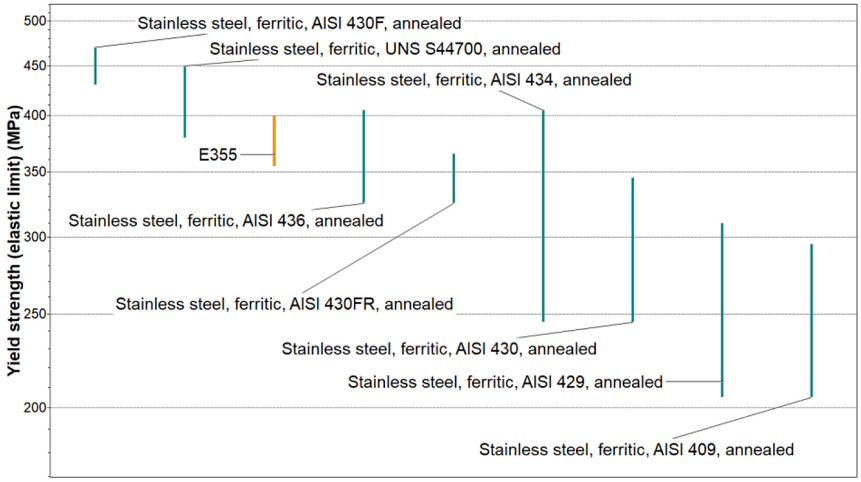

Figure 2. Yield strength comparison of ferritic stainless steels with E355 steel

(FEM) using the ADINA System software (Figure 3). Due to the axial symmetry of the welded components, a thermomechanical, axisymmetric and two-dimensional (2D) model of friction welding was developed, taking into account the connection of mechanical loads and thermal loads.

In the analysed case, the tube part rotates and is pressed with its front surface against the stationary washer. In the numerical model, the mesh was made using a 4-node quadrangular elements with displacement and temperature coupling. The distribution of the temperature field in axisymmetric elements is described by the Fourier Equation in the following form Eq. 1:

$$\frac{\partial}{\partial r}\left(\lambda\frac{\partial T}{\partial r}\right)+\lambda\frac{1}{r}\frac{\partial T}{\partial r}+\frac{\partial}{\partial z}\left(\lambda\frac{\partial T}{\partial z}\right)+ +\frac{1}{r^2}\frac{\partial}{\partial\varphi}\left(\lambda\frac{\partial T}{\partial\varphi}\right)+q_v=c_p\rho\frac{\partial T}{\partial t} \quad (1)$$

where: λ – thermal conductivity coefficient, q_v – heat generation rate per volume unit, p– the density of the medium at temperature T, c_p – specific heat.

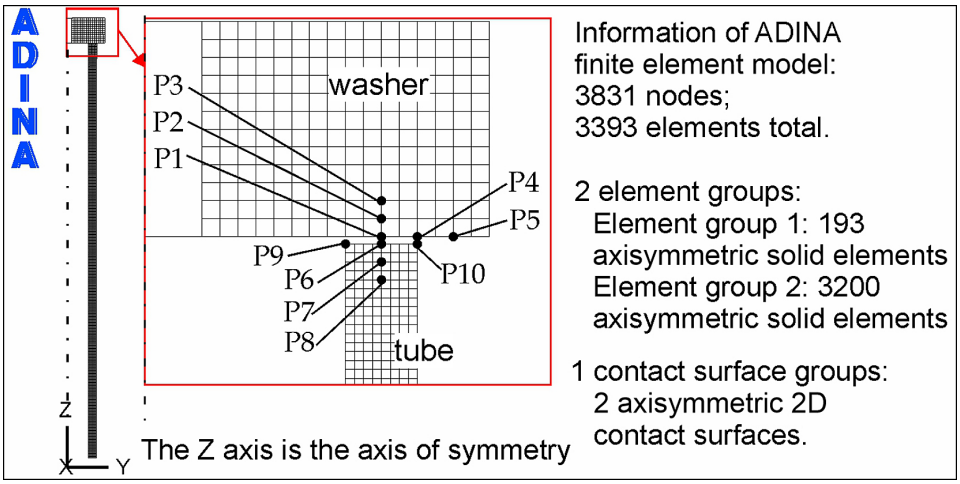

Figure 3. Numerical model of welding process

Assuming like in [19] that no heat is released in the considered volume and due to the uniform temperature distribution in any axial section of the sample, Equation 1 can be presented in a simplified form Equation 2:

$$\frac{\partial}{\partial r}\left(\lambda\frac{\partial T}{\partial r}\right)+\lambda\frac{1}{r}\frac{\partial T}{\partial r}+\frac{\partial}{\partial z}\left(\lambda\frac{\partial T}{\partial z}\right)=c_p\rho\frac{\partial T}{\partial t} \quad (2)$$

In the general case, temperature is a function of both r and z coordinates and time t. Therefore, the solution of the above Equation is a two-step solution: solving the steady-state Equation, and then adapting the solution obtained in the first step to the conditions of the transient process using discretization of the time variable.
For a steady process, Eq. 2 can be written:

$$\frac{\partial}{\partial r}\left(\lambda\frac{\partial T}{\partial r}\right)+\lambda\frac{1}{r}\frac{\partial T}{\partial r}+\frac{\partial}{\partial z}\left(\lambda\frac{\partial T}{\partial z}\right)=0 \quad (3)$$

$$\frac{\lambda}{r}\left(r\frac{\partial^2 T}{\partial r^2}+\frac{\partial T}{\partial r}\right)+\lambda\frac{\partial^2 T}{\partial z^2}=0 \quad (4)$$

Because:

$$\frac{\partial}{\partial r}\left(r\frac{\partial T}{\partial r}\right)=|uv'+u'v|=r\frac{\partial^2 T}{\partial r^2}+\frac{\partial T}{\partial r} \quad (5)$$

is received:

$$\frac{\lambda}{r}\frac{\partial}{\partial r}\left(r\frac{\partial T}{\partial r}\right)+\lambda\frac{\partial^2 T}{\partial z^2}=0 \quad /r \quad (6)$$

$$\frac{\partial}{\partial r}\left(\lambda r\frac{\partial T}{\partial r}\right)+\frac{\partial}{\partial z}\left(\lambda r\frac{\partial T}{\partial z}\right)=0 \quad (7)$$

Physical conditions impose certain boundary conditions:

- the value of T is given at the edge of the region $T = T_B$ or:

$$\lambda\frac{\partial T}{\partial r}l_r+\lambda\frac{\partial T}{\partial z}l_z+q+\alpha T=0 \quad (8)$$

where: l_r, l_z – the directional cosines of the exterior normal to the surface bounding the area, q – the heat flux transferred to the material as a result of the friction work, a – heat transfer coefficient.

Equation 1 together with the boundary conditions clearly define the problem of temperature changes in the elements during the entire welding process. The use of the finite element method to solve heat flow problems requires the representation of Equation 1 including boundary conditions via the calculus of variations. It follows from Euler's theorem that if the integral:

$$\chi(T)=\iint_V f\left(r,z,T,\frac{\partial T}{\partial r},\frac{\partial T}{\partial z}\right)drdz \quad (9)$$

must be minimized in a region bounded by V, then a necessary and sufficient condition to reach the minimum is that the unknown function $T(r,z)$ satisfies the following differential Equation:

$$\frac{\partial}{\partial r}\left\{\frac{\partial f}{\partial\left(\frac{\partial T}{\partial r}\right)}\right\}+\frac{\partial}{\partial z}\left\{\frac{\partial f}{\partial\left(\frac{\partial T}{\partial z}\right)}\right\}=0 \quad (10)$$

within the same region, assuming that T satisfies the same boundary conditions in both cases.

It can be stated that the demand to solve Equation 1 is equivalent to obtaining the minimum value of the integral extended over the entire area:

$$\chi=\iint_V\left[\frac{1}{2}\left\{r\lambda\left(\frac{\partial T}{\partial r}\right)^2+r\lambda\left(\frac{\partial T}{\partial z}\right)^2\right\}\right]drdz \quad (11)$$

assuming that T satisfies the same boundary conditions.

Simultaneously imposing boundary conditions (a) and (b) on the examined function is impractical and sometimes difficult to implement. To avoid this, it is preferable not to extend the boundary conditions to those areas of the boundary where condition (b) holds, but to add to the functional from Equation 11 another integral relating to the boundary surface,

which, after minimization, automatically leads to the boundary condition. In the general notation of Euler's Equation, this is the integral:

$$\int_S \left(qT + \frac{1}{2}\alpha T^2\right) dS \tag{12}$$

$$\chi = \int_V \left[\frac{1}{2}\left\{r\lambda\left(\frac{\partial T}{\partial r}\right)^2 + r\lambda\left(\frac{\partial T}{\partial z}\right)^2\right\}\right] drdz + \int_S \left(qT + \frac{1}{2}\alpha T^2\right) dS \tag{13}$$

where S is the surface where the boundary condition (b) holds.

Optimization of the functional (11) in the domain of discrete functions consists in replacing the continuous real temperature distribution functions $T(r,z)$ by their discrete equivalents:

$$T = \left[N_i, N_j, \dots\right] \begin{Bmatrix} T_i \\ T_j \\ . \\ . \\ . \end{Bmatrix} = [N]\{T\}^e \tag{14}$$

where: $\{T\}$ is a vector of nodal temperature values, and $[N]$ is a matrix of shape functions whose form depends on the type of finite elements.

The adopted method of discretization allows to determine the values of temperature derivatives with respect to the r and z coordinates.

If the unknown function T is defined element by element, we can approximate the minimization of the functional (13). The necessary condition for the minimum of the functional are zero values of partial derivatives of the functional with respect to the vector of nodal temperatures. In general, the share of each element is calculated:

$$\frac{\partial \chi}{\partial T_i} = \int_{V^e} \left\{r\lambda\frac{\partial T}{\partial r}\frac{\partial}{\partial T_i}\left(\frac{\partial T}{\partial r}\right) + r\lambda\frac{\partial T}{\partial z}\frac{\partial}{\partial T_i}\left(\frac{\partial T}{\partial z}\right)\right\} drdz + \int_{S^e}\left(q\frac{\partial T}{\partial T_i} + \alpha T\frac{\partial T}{\partial T_i}\right) dS \tag{15}$$

with the second integral being used only if the element has an outer surface where a boundary condition of type (b) prevails.

Whereas:

$$\frac{\partial T}{\partial r} = \left[\frac{\partial N_i}{\partial r}, \frac{\partial N_j}{\partial r}, \dots\right]\{T\}^e \tag{16}$$

$$\frac{\partial}{\partial T_i}\left(\frac{\partial T}{\partial r}\right) = \frac{\partial N_i}{\partial r}\ ,\ \frac{\partial T}{\partial T_i} = N_i \tag{17}$$

We get directly for the whole item:

$$\frac{\partial \chi^e}{\partial (T)^e} = [h]^e\{T\}^e + \{F\}^e \tag{18}$$

where: $[h]^e$ is defined by:

$$h_{ij}^e = \int_{V^e}\left\{r\lambda\frac{\partial N_i}{\partial r}\frac{\partial N_j}{\partial r} + r\lambda\frac{\partial N_i}{\partial z}\frac{\partial N_j}{\partial z}\right\} drdz \tag{19}$$

and

$$F_i{}^e = \int_{S^e} qN_i dS + \left(\int_{S^e}[N]\alpha N_i dS\right)\{T\}^e \tag{20}$$

So it is for the entire area:

$$\frac{\partial \chi}{\partial \{T\}} = [H]\{T\} + \{F\} = 0 \tag{21}$$

where:

$$H_{ij} = \sum h_{ij}^e \tag{22}$$

$$F_i = \sum F_i^e \tag{23}$$

A model of Coulomb friction was assumed, as a result of which heat is generated on the contact surfaces. The amount of heat released depends on the relative linear speed of the friction surfaces v, the coefficient of friction depending on the temperature $\mu(T)$ and the contact force in the friction phase F_f Equation 24.

$$q = \mu(T) \times F_f \times v \tag{24}$$

Figure 4 shows the dependence of the friction coefficient on temperature assumed in the FEM analysis. According to the presented dependence, in the low temperature range (up to 400 °C) there is a constant coefficient of friction μ = 0.1 and close to zero μ = 0.01 above the melting point of the welded materials.

In the analysis, an elastic-plastic model of the materials with strain hardening was assumed. The course of the yield strength was assumed as a function of temperature (Figures 5 and 6). The thermal model takes into account heat conduction between the welded parts, parts and the machine tool, as well as heat exchange (radiation and convection) with the environment. In the calculations, the initial temperature of the welded parts was assumed equal to the ambient temperature Ta = 20 °C. Table 4 and Figure 7 present selected parameters of the RFW process for the analysed joint, taking into account the properties of the joined materials of E355 as well as X6CrMo17-1 steel grades.

In the basic assumption, which involved welding both components made of E355 steel, the welding time was 4 s. This time resulted from the type of material being welded, and therefore its properties, and the need to conduct the process on an automatic production line. Changing the washer material allowed the welding time to be reduced by one second, which increased production efficiency by 25%. Due to the short welding time, a relatively high rotational speed was used.

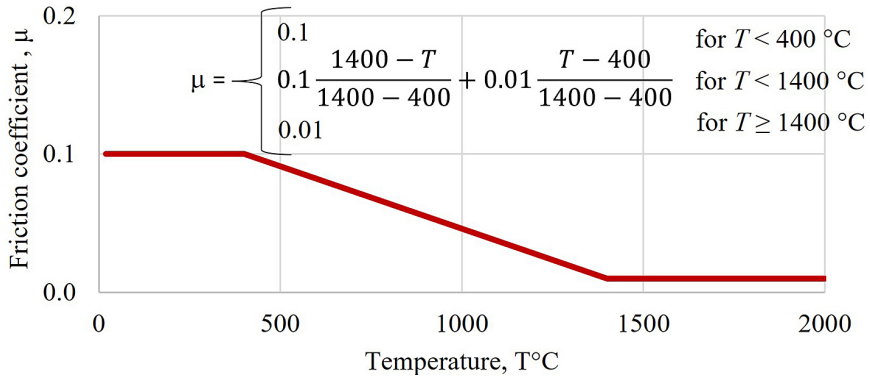

Figure 4. Dependence of coefficient of friction on temperature for the fiction pair E355 -X6CrMo17-1

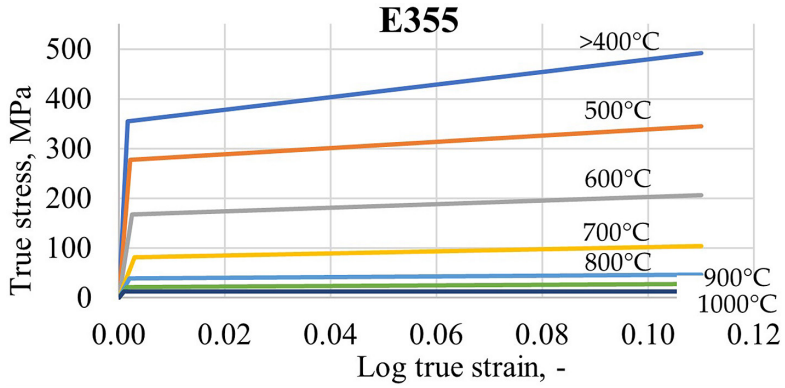

Figure 5. True strain – stress relationship at elevated temperatures of E355 steel

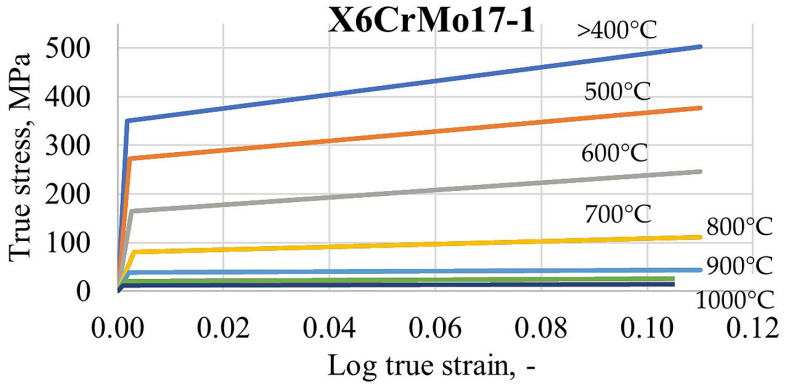

Figure 6. True strain – stress relationship at elevated temperatures of X6CrMo17-1 steel

RESULTS AND DISCUSSION

Temperature distributions in the welded components after 1, 1.5, 2 and 3 s were shown in Figure 8. After 1 s, the temperature increases in both joined components. The maximum temperature of 970 °C occurred in the area of the friction surface. Up to 0.5 s, when the pressing force increased, the temperature increase in the connection took place in the area of the friction surfaces, on the inner side (located closer to the axis of rotation). After 1 s, a symmetrical temperature distribution was observed in the tube with respect to the vertical axis passing through point P6. In the washer, however, the temperature was still higher on the inside than on the outside.

After 1.5 s, the temperature increased to a maximum of 1050 °C, which is about 75% of the melting point of the considered steel grades. The tube continued to show a symmetrical temperature distribution with respect to the vertical axis. On the other hand, in the washer the temperature reached

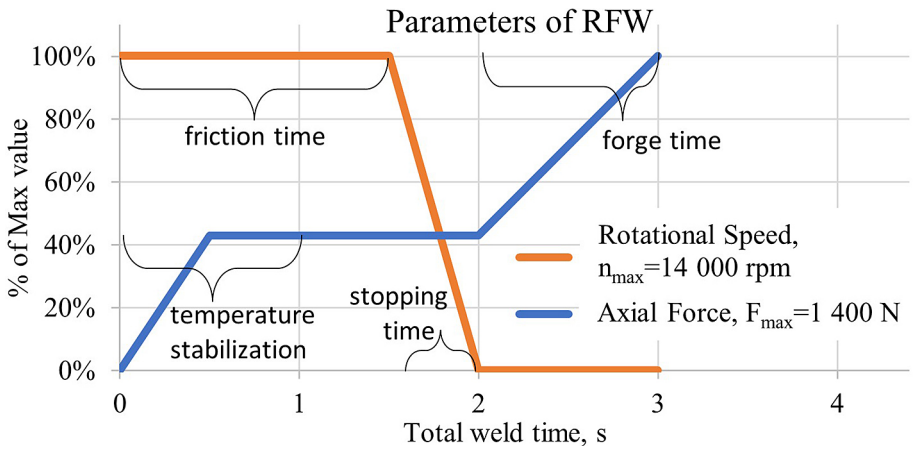

Figure 7. Parameters of RFW process adopted in numerical model

Table 4. Parameters of RFW process adopted in numerical model

Rotational speed, rpm	Friction force, N	Upset force, N	Total time, s
14 000	600	1 400	3.0

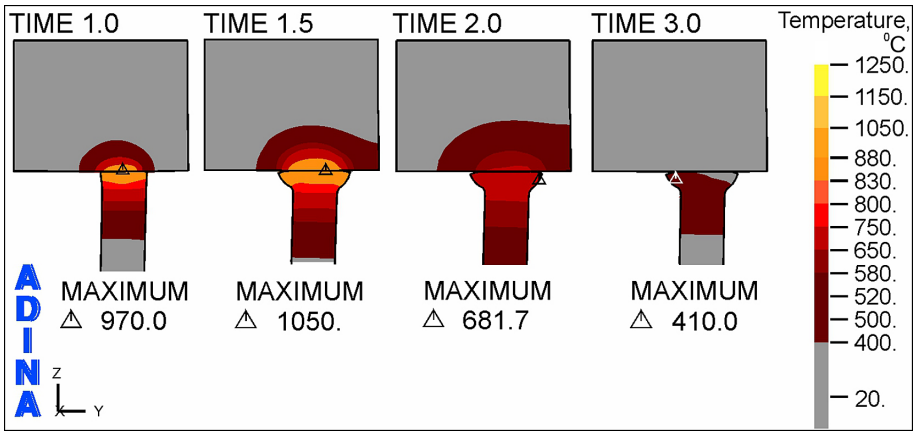

Figure 8. Temperature distribution in joint area

higher values on the outside. This is due to the direction of the temperature increase and the smaller volume of the washer material on the outer side in relation to the incoming tube. After 2 s, when the rotational speed decreased to 0 rpm, but the axial force increased, the temperature levelled out in the weld area. After 3 s, the temperature did not exceed 410 °C. Except that a higher temperature was observed in the tube than in the washer. The volume of the washer is smaller than that of the tube, the thermal conductivity of X6CrMo17-1 steel is almost half that of E355 steel.

Analysing Figure 9, it was observed that point P1 heats up the fastest. The reason is the fact that point P1 is located on the friction surface, in its center. After about 0.8 s, the temperature at point P1 stabilized. At the same time, the highest temperature in the entire washer volume occurred at this point and amounted to about 1050 °C. It was observed after 1.5 s, i.e. after the end of the friction stage. After exceeding 1.5 s, i.e. after switching off the rotation, the temperature at point P1 decreases.

At the next points P2 and P3, which are located on the same Y coordinate that P1 point, but move away from the Z axis, into the washer volume, the maximum temperature values are lower, 820 and 655 °C, respectively. The character of the curve at point P4 is similar to the curve P1. However, at point P4 the temperature increases more slowly than at P1 and its maximum is equal to 955 °C.

Among the analysed points located in the tube (Figure 10), the highest temperature was observed at point P6, i.e. located on the friction surface, in the middle of its width. The maximum value was

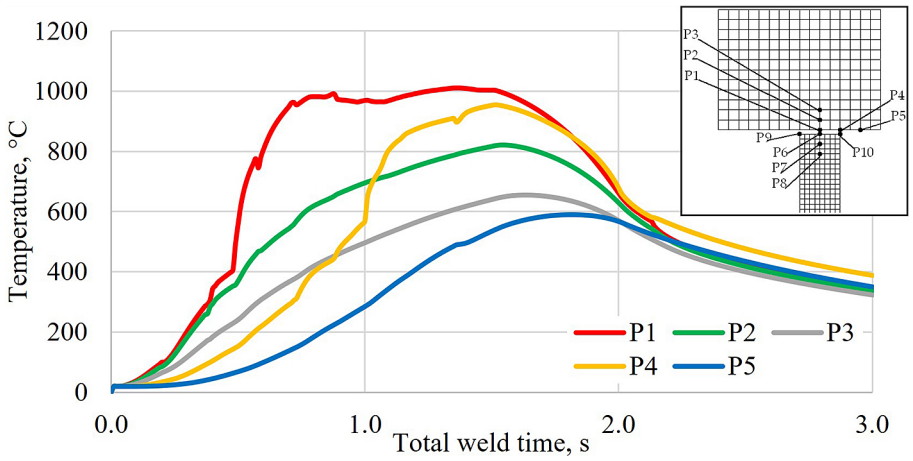

Figure 9. The course of temperature as a function of time at points P1–P5 in the washer

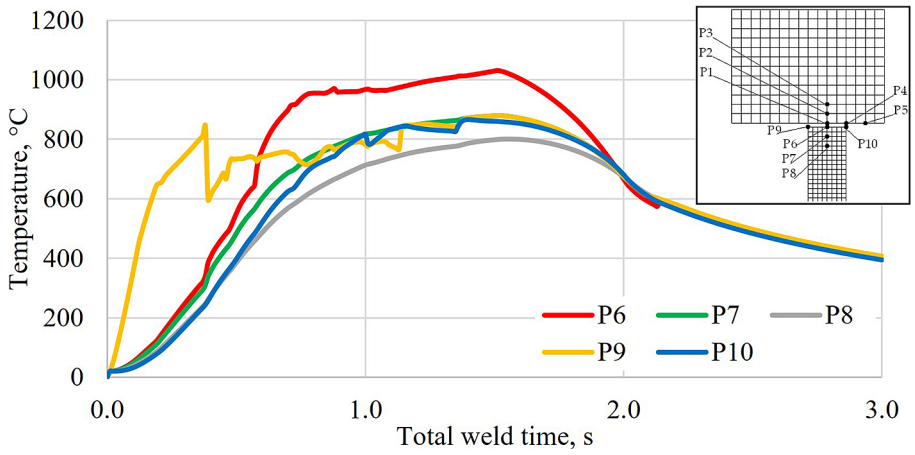

Figure 10. The course of temperature as a function of time at points P6–P10 in the tube

1030 °C. The extreme occurred after 1.5 s, i.e. in the last step, where the rotational speed was maximum, so the maximum temperature is 20 °C lower than in the washer. This is due to the thermal conductivity of E355 steel, which is almost twice as hight as that of X6CrMo17-1 steel and the volume of the tube is bigger than that of the washer.

The fastest increase of temperature in relative to time was observed at point P9, which is located on the friction surface, but on its inner side, where the circumferential speed is the smallest. This is due to the fact that the contact between the friction surfaces appears from the inside of the tube (P9) and increases towards the outside (P10). The temperature at this point reached a maximum of 844 °C after about 0.4 s. The temperature then dropped to about 600 °C. It stabilized after about 0.5 s, when the downforce stabilized at the same time. It is also worth paying attention to the temperature course at point P10, which, like P6 and P9, is also located on the friction surface. The maximum temperature value at P10 is similar to P9 and amounts to 864 °C, but its increase is definitely slower than at P9. The temperature extreme at this point was reached after 1.4 s.

The work proposes a numerical model for process design. The input data to the model was based on literature. At the moment, the simulation results have not been verified by experimental tests. At a further stage of research, experimental verification of the model is planned, after the research site is made available by an industry partner.

The welding process, and therefore the quality of the joint, is influenced by the process parameters (their mutual combination), which depend not only on the type of welded materials, but also on the geometry and dimensions of the joined components as well as the technological requirements. There are many papers presenting the numerical modeling of the rotational friction welding process, taking into account various friction models, different boundary conditions and different material models. The authors of the works present the results of calculations most often in the form of temperature and stress field

distributions in the joint area for the established welding process parameters.

There are no research results in the literature on the RFW welding process of components with a geometry similar to that presented in this work, made of E355 and X6CrMo17-1 steel, carried out at such a high rotational speed (14,000 rpm) and short total welding time (3 s).The paper [20] presents the numerical simulations results of rotational friction welding bars with a diameter of 25 mm made of SUS304 steel. The numerical model of the process was verified experimentally for a rotational speed of 900 rpm and a pressure of 80 MPa. Based on the obtained simulation results of the temperature and stress field distribution and the results of strength tests, the authors of the research determined the minimum welding time (1.5–2.9 s) necessary to create a good-quality joint in the rotational speed range of 500–2500 rpm. Additionally, the authors of the study [20] showed that the last stage of the process, corresponding to the formation of the flash, which is formed at constant temperature and stress fields, has a negligible impact on the strength of the joints.

The authors of paper [21] presented the results of tests on RFW samples made of SUS304 and A286 stainless steels. Based on the welding process of pipe elements, models of the friction coefficient as a function of the linear friction velocity, pressure and temperature were developed. According to the authors of the paper, the joint formation time for samples made of SUS304 steel was approximately 5 s and was approximately independent of the rotational speed, while for samples made of A286 steel the joint formation time ranges from 5 s to 20 s and increases with the rotational speed in the range of 500 rpm to 2000 rpm/min.

Results of the numerical simulation of the friction welding process of pipes with an external diameter of 35 mm and a wall thickness of 7 mm made of various types of materials, i.e. austenitic stainless steel TP347HFG and ferritic stainless steel alloy HiPerFer (Hiperfer ferritic alloy) were presented in [22]. The authors of the research determined the optimal set of process parameters based on the obtained experimental results and calculated equivalent stresses, total deformations and temperature distribution in the contact area. The authors showed that the greatest influence on temperature was exerted by pressure and time in the friction phase, and to a lesser extent by rotational speed and pressure in the upsetting phase. According to the authors, the upsetting pressure and rotational speed have a greater impact on the amount of deformation. The optimal process parameters were access as follows: friction pressure 80 MPa, friction time 5 s, forging pressure 165 MPa, forging time 5 s, speed 1500 rpm.

CONCLUSIONS

Numerical simulations of the process allow the determination of temperature fields. Thanks to this, it is possible to solve a number of technological problems occurring during RFW welding processes already at the design stage. Numerical calculations also allow to analyse the influence of most parameters on the course of the RFW process and the quality of joints. A two-dimensional axisymmetric numerical model of the RFW process of components in the form of a pipe with and washer made of E355 steel and X6CrMo17-1 steel, respectively, was developed. The simulations performed made it possible to determine the temperature fields in the cross-section of the connected components. The following conclusions can be drawn from the study:

- the obtained results were influenced by the defined process parameters, the adopted material models, the friction model and the value of the heat transfer coefficient on the contact surface between the welded components,
- during the RFW process, the uneven temperature distribution was observed in the cross-section of the joint area which changes in subsequent welding stages with changes of the time and other assumed parameters (asymmetric distribution of temperature fields results from the difference in thermal properties of the base materials and the varied geometry of the joined components),
- for the assumed process parameters: rotational speed of 14,000 rpm, friction time of 1.5 s and friction force of 600 N, the peak temperature occurred in the center of the friction surface on the washer surface at the end of the friction phase and amounted to 1050 °C,
- the maximum temperature value observed in the joint cross-section throughout the welding process was approximately 75% of the melting point of the considered steel grades,
- during the upsetting stage, accompanied by the increase of force to the upsetting force value of 1400 N, the gradual decrease in temperature was observed, which after the total welding time of 3 s was stabilized at a level of 400 °C.

The results of the temperature analysis are one of the most important parameters for the implementation of subsequent calculations, such as the calculation of structural changes, hardness, residual stresses and deformations.

Acknowledgements

The authors are grateful to the Czestochowa University of Technology, for the financial support granted under research project BS/PB-500-301-1/23 Z.3.

REFERENCES

1. Klimpel A. Metal and thermoplastic welding technologies. Gliwice: Wydawnictwo Politechniki Śląskiej, 1999.
2. Michalski R., Kamiński Z. Friction welding. Warszawa: Wydawnictwa Naukowo-Techniczne, 1975.
3. Ambroziak A. Friction welding of materials with different properties. Wrocław: Oficyna Wydawnicza Politechniki Wrocławskiej, 2011.
4. Pietras A., Bogucki R. Characteristics of friction welding of metal construction elements. Szybkobieżne Pojazdy Gąsiennicowe 2005, 21(1): 1–9.
5. Bhate S.S., Bhatwadekar S.G. A Literature Review of research on rotary friction welding. Int. J. Innovative Technol. Res. 2016, 4(1): 2601–2064.
6. Szczucka-Lasota B., Węgrzyn T. Modern materials and innovative welding technology used in the construction of antenna mounts. Sci. J. Sil. Univ. Technol., Ser. Transp. 2022, 115: 175–82. https://doi.org/10.20858/sjsutst.2022.115.12
7. Szczucka-Lasota B., Węgrzyn T., Jurek A. Aluminum alloy welding in automotive industry. Transp. Probl. 2020, 15(3): 67–78. https://doi.org/10.21307/tp-2020-034
8. Senthil Murugan S., Sathiya P., Noorul Haq A. Rotary friction welding and dissimilar metal joining of aluminium and stainless steel alloys. Awet 2021, 32: 85–92. https://doi.org/10.35219/awet.2021.11
9. Moghadasi K., Mohd Isa M.S., Ariffin M.A., Mohd Jamil M.Z., Raja S., Wu B. et al. A review on biomedical implant materials and the effect of friction stir based techniques on their mechanical and tribological properties. J. Mater. Res. Technol. 2022, 17: 1054–121. https://doi.org/10.1016/j.jmrt.2022.01.050
10. Balta B., Arici A.A., Yilmaz M. Optimization of process parameters for friction weld steel tube to forging joints. Mater. Design. 2016, 103: 209–22. https://doi.org/10.1016/j.matdes.2016.04.072
11. International Standard. Welding - Friction welding of metallic materials (ISO 15620-2000). Printed in Switzerland: The International Organization for Standardization (ISO), 2000.
12. Humphreys B.A. A practical guide to friction welding, 2004.
13. Skowrońska B., Bober M., Kołodziejczak P., Baranowski M., Kozłowski M., Chmielewski T. Solid-state rotary friction-welded tungsten and mild steel joints. Appl. Sci. 2022, 12(18): 9034. https://doi.org/10.3390/app12189034
14. Służalec A. Thermal effects in friction welding. Int J Mech Sci 1990, 32(6): 467–78. https://doi.org/10.1016/0020-7403(90)90153-A
15. Schmicker D., Persson P.-O., Strackeljan J. Implicit Geometry Meshing for the simulation of Rotary Friction Welding. J. Comput. Phys. 2014, 270: 478–89. https://doi.org/10.1016/j.jcp.2014.04.014
16. Tang T., Shi Q., Lei B., Zhou J., Gao Y., Li Y., Zhang G., Chen G. Transition of interfacial friction regime and its influence on thermal responses in rotary friction welding of SUS304 stainless steel: A fully coupled transient thermomechanical analysis. J. Manuf. Process. 2022, 82: 403–14. https://doi.org/10.1016/j.jmapro.2022.08.016
17. Lacki P., Adamus J., Więckowski W., Motyka M. A New method of predicting the parameters of the rotational friction welding process based on the determination of the frictional heat transfer in Ti grade 2/AA 5005 joints. Materials (Basel) 2023, 16(13). https://doi.org/10.3390/ma16134787
18. ANSYS, Granta EduPack 2022 R1 Version: 22.1.2: Getting Started with Granta EduPack. 2022.
19. Lacki P. The influence of hardening layers and lubricants on the distribution of stresses and strains in forging dies: PhD thesis: Politechnika Częstochowska Wydział Budowy Maszyn, 1999.
20. Jin F., Li J., Du Y., Nan X., Shi J., Xiong J., Zhang F. Numerical simulation based upon friction coefficient model on thermo-mechanical coupling in rotary friction welding corresponding with corona-bond evolution. J. Manuf. Process. 2019, 45: 595–602. https://doi.org/10.1016/j.jmapro.2019.08.001
21. Jin F., Li J., Liu P., Nan X., Li X., Xiong J., Zhang F. Friction coefficient model and joint formation in rotary friction welding. J. Manuf. Process. 2019, 46: 286–97. https://doi.org/10.1016/j.jmapro.2019.09.008
22. Mattie A.A., Ezdeen S.Y., Khidhir G.I. Optimization of parameters in rotary friction welding process of dissimilar austenitic and ferritic stainless steel using finite element analysis. Advances in Mechanical Engineering 2023, 15(7). https://doi.org/10.1177/16878132231186015